Reliable neuronal logic devices from patterned hippocampal cultures

OFER FEINERMAN[1]*, ASSAF ROTEM[2]*† AND ELISHA MOSES[2]

[1]Memorial Sloan-Kettering Cancer Center, Computational Biology Center, New York 10065, USA
[2]Weizmann Institute of Science, Physics of Complex Systems, PO Box 26, Rehovot, 76100, Israel
*These authors contributed equally to this work
†e-mail: assaf.rotem@weizmann.ac.il

Published online: 12 October 2008; doi:10.1038/nphys1099

Functional logical microcircuits are an essential building block of computation in the brain. However, single neuronal connections are unreliable, and it is unclear how neuronal ensembles can be constructed to achieve high response fidelity. Here, we show that reliable, mesoscale logical devices can be created *in vitro* by geometrical design of neural cultures. We control the connections and activity by assembling living neural networks on quasi-one-dimensional configurations. The linear geometry yields reliable transmission lines. Incorporating thin lines creates 'threshold' devices and logical 'AND gates'. Breaking the symmetry of transmission makes neuronal 'diodes'. All of these function with error rates well below that of a single connection. The von Neumann model of redundancy and error correction accounts well for all of the devices, giving a quantitative estimate for the reliability of a neuronal connection and of threshold devices. These neuronal devices may contribute to the implementation of computation *in vitro* and, ultimately, to its understanding *in vivo*.

Neuronal circuits can carry out complex computations reliably; the right connectivity matrix will enable the performance of difficult calculations[1] on surprisingly short timescales and with little error. The major potential for errors lies in the noisy synaptic connections of the network rather than in the single neuron responses[2]. In a seminal paper, von Neumann[3] showed how reliability may be restored to a computing device despite unreliable connections through redundancy of computing units and the multiplexing of their connections. In the brain, redundancy is indeed thought to exist at all levels, but the way in which it is incorporated in living neural structures is still unknown. Although *in vitro* neuronal cultures are probably the natural set-up to investigate this, controlling the connections in a living neural network has not been feasible until now.

Activity in cultured neural networks *in vitro* is characterized by synchronized large-scale network bursts in which practically all of the neurons participate, each firing a number of spikes[4,5]. The bursts are thought to be analogous in some ways to pulses that propagate in the brain[5,6]. The activity percolates throughout the culture[7], starting at sources or initiation sites[8] that are still not well identified. A relatively long refractory time occurs due to the depletion of resources[8], leading to burst frequencies in the range of 1–0.02 Hz (ref. 9).

Significant advances towards the creation of neuronal devices have been made by patterning connections between neurons, thus creating computational networks[10–14]. Recently, cultures of neurons constrained to grow on a one-dimensional pattern have emerged as a simplified network that can be precisely controlled and quantitatively understood[15,16]. One-dimensional cultures offer a number of significant advantages. First, connections are ordered and causal—signals can propagate along only one path and are thus easily monitored under the microscope using a calcium-sensitive fluorescent dye (see the Methods section). Second, the density of neurons can be controlled by thinning the lines. Finally, intermediate forms such as triangles allow a mixture of one- and two-dimensional structures, leading to convergence of axons onto a critical region. Here, we use these techniques to create several configurations of neurons that carry out logical functions.

DEVICES

Three devices for computation were constructed, as shown in Fig. 1. Activity was either stimulated externally[17] or spontaneously generated (with no measured differences) at a localized area defined as the 'input' and monitored at a different part of the culture defined as the 'output'. The basic unit is a simple threshold component (Fig. 2a), which needs sufficiently high amplitude at the input for the output to fire. In Fig. 2a, only bursts in which the amplitudes in region 1 were greater than 80% of the maximum amplitude (red line in the figure) propagated to region 2. One example of an error occurs at $t = 60$ s. The graph of the input versus output amplitudes (right panel) summarizes 89 bursts in 4 experiments. Two of the 33 bursts that propagated through were sub-threshold errors. Three of the 56 bursts that were blocked were super-threshold errors, giving a total error rate of 6%.

Assembling two threshold components in parallel creates the AND gate (Fig. 2b), which allows the two input signals to propagate only if they are coincidental. Localized application[17] of the sodium ion channel blocker tetrodotoxin (TTX) was used to disconnect inputs 1 and 2 (red arrow in the figure). When this was done, bursts from only one input (1 or 2) did not activate output region 3 (corresponding to the AND truth table entries $1 \wedge 0 = 0$, $0 \wedge 1 = 0$). Shutting off the TTX application enabled simultaneous activity in both inputs and the subsequent excitation of the output

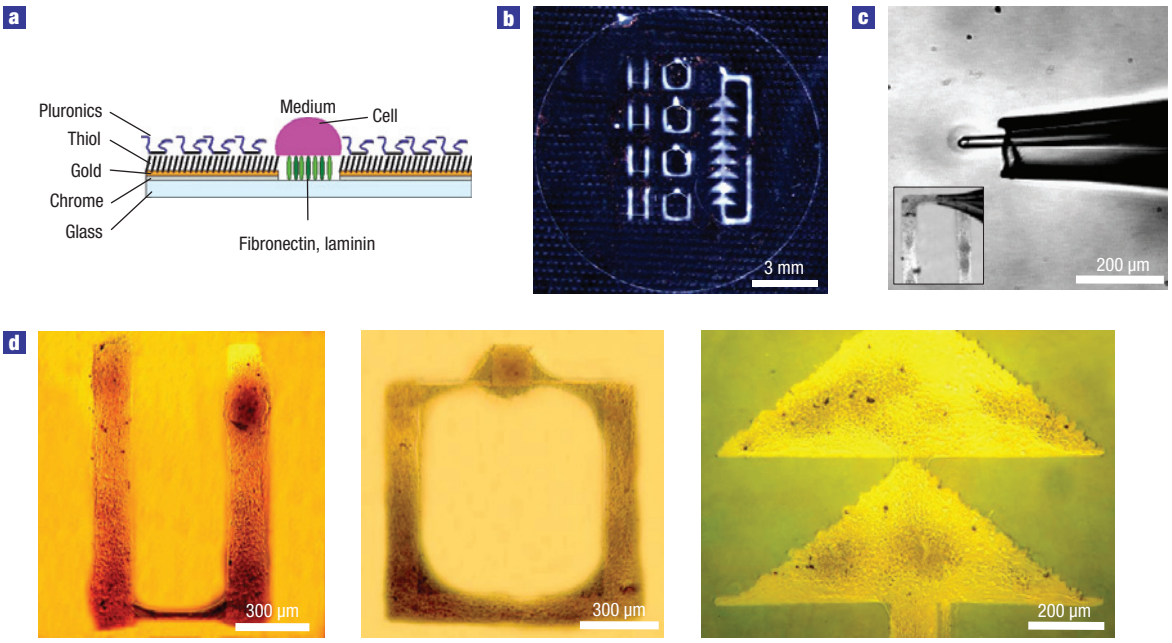

Figure 1 Patterning neuronal cultures. a, The glass coverslip is first coated by a cell-repellent surface. Specific patterns are etched through this surface and the coverslip is recoated by fibronectin and laminin (see the Methods section). **b**, Nine separate neuronal devices patterned on a single 13 mm coverslip (4 thresholds on the left column, 4 AND gates on the centre column and on the right a composite diode consisting of 8 daisy-chained triangles). Dark-field illumination, bright areas are concentrations of neurons. **c**, Local drug application using a specially designed double-pipette system. The double pipette applies its contents only to a confined volume (grey cloud around the tip of the small pipette). The pipette is placed directly over the targeted neuronal area (inset). **d**, Bright-field images of the three devices. Left: threshold, centre: AND gate, right: a diode.

(corresponding to $1 \wedge 1 = 1$). Time differences between the inputs as large as 100 ms still elicited a response in the output. To summarize the dependence of amplitudes, we present a three-dimensional plot of the output amplitude as a function of both amplitudes from inputs 1 and 2. The four states of an AND gate are all accessible, allowing a functional AND gate with a measured error rate of 6%.

The diode (Fig. 2c) uses an asymmetric variation on the threshold component, which gives preference to input signals with one specific direction of propagation. As shown in Fig. 2c, only forward propagation is enabled, from region 2 to region 1. The inset shows a typical forward propagation occurring at $t = 33$ s. The graph of input versus output amplitudes demonstrates that signals propagate forward with nearly perfect reliability, whereas those propagating backwards are blocked with high probability, giving a total error rate of 8%. Errors can also occur if a spontaneous burst at region 2 renders it refractory and thus non-responsive to a closely succeeding burst propagating from region 1. For the spontaneous firing rate of our cultures, this rarely happens, contributing about 1% error.

These logic devices can be very reliable, with virtually no error in some devices and 7% error averaged over all devices. The functionality of these devices is dictated by their connectivity patterns. The devices rely on patterning transitions from a relatively wide line (~170 μm thick) where cell bodies reside, to a thin section (~50 μm thick). Because of the weak adhesion characterizing our patterned samples, only axons traverse this thin line[15] (for details see Supplementary Information). On its own, the thin section constitutes a threshold device. Low-amplitude activity cannot propagate through the barrier and is effectively blocked. A key observation that we will make is that the number of axons on the thin section provides an adjustable barrier for signal propagation.

INFRASTRUCTURE

We have shown previously that hippocampal neurons growing on lines thinner than 200 μm can be treated as a one-dimensional culture, because the synaptic input basin is of the order of the width of the line[15]. This collapses the small dimension of the line and enables it to be referred to as a one-dimensional system. Although growing neurons on triangular patterns (see below) does not maintain the constraints of one-dimensional systems, the directional control over axons remains.

An image with cells transfected with green fluorescent protein (GFP) in Fig. 3a shows some of the axons that traverse the threshold (GFP transfection efficiency was 1%). The density of axons along the thin sections is about four times lower than in the thick section. Given that only 1% of the neurons are transfected, there are on average $M_{thr} = 120$ cells that send axons across the threshold barrier (see Supplementary Information). A threshold component can also be created pharmacologically by a dilute (300 nM) localized application[17] of TTX on a thick line (data not shown).

Figure 3b shows GFP-transfected cells in a directional transmission line (or 'diode'). On regular transmission lines, axons will grow in both directions with no preference. The diode breaks this symmetry by geometrically constraining the neurons, making use of the axons' rigidity and forcing them to propagate preferentially in one direction.

In Fig. 3b, triangular white frames mark the borders of three consecutive triangles that make two 'daisy chained' diodes. Figure 3c focuses on the axons, which branch extensively and may extend more than 3 mm away from the cell body. Axons keep their direction and make few turns, advancing in long stretches that are parallel to the pattern borders. The triangular structure creates a 'funnel' effect, so that when axons approach the wall they do so

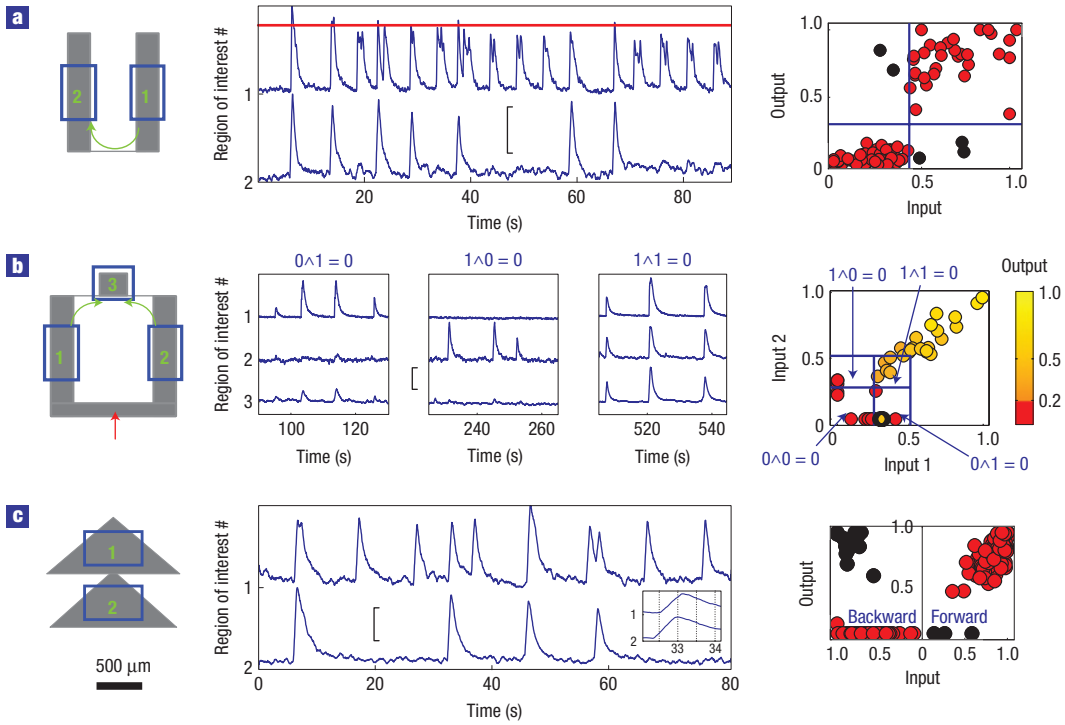

Figure 2 Function of the neuronal devices. a, Left: schematic diagram of threshold component. Centre: traces of fluorescence intensity. All signals initiated in region 1. The red line indicates the threshold value. Right: input amplitude versus output amplitude of all bursts. **b**, Left: schematic diagram of AND gate. The red arrow indicates the focus of TTX application (see text). Centre: time traces of fluorescence intensity exemplify the function of the AND gate. Right: plot of amplitudes from inputs 1 (x axis) and 2 (y axis) versus the output amplitude (colour code). Red and yellow shades represent sub-threshold and super-threshold output events respectively (51 bursts in one experiment). Blue lines separate the four states of an AND gate. Three of the 27 bursts that propagated through the gate were sub-threshold errors in one input region. **c**, Left: schematic diagram of neuronal diode. Centre: time traces of fluorescence intensity from two consecutive triangles demonstrate the diode's function. Inset: typical forward propagation at $t = 333$. Right: input versus output amplitudes (234 bursts in six experiments). Forward propagation is in the right side of the graph, whereas backward propagation is in the left. Three of the 132 forward bursts did not propagate through and 16 of the 102 backward bursts (with exceptionally high input amplitude) succeeded to propagate through. In all devices, black circles denote errors. Amplitudes given are the peaks of the bursts f, rescaled per region by the maximum f_{max} and minimal f_{min} peak values, $A = (f - f_{min})/(f_{max} - f_{min})$. All events shown are spontaneous network bursts. Vertical bars represent 50% of the maximum amplitude in each trace. Amplitudes lower than 20% tend to decay and were considered as propagation failures.

more often at an angle that leads them along the boundary towards the apex of the triangle than towards its base. The ratio in the lower crossing is one cell sending axons forward versus one cell backwards, whereas in the upper crossing three cells cross forward and only one goes backwards (see below).

AXON GROWTH MODEL

Two rules for the advance of axons can be extracted from the GFP images: axons do not grow outside the patterned area, and because their measured persistence length ($420 \pm 50\,\mu m$) is on the scale of the triangle dimensions, they make only few and small turns (Fig. 3d). Using these two approximate laws, we have been able to simulate the axonal growth. In the simulation, axons originate at the locations in which cells were observed in the GFP images. They advance to neighbouring lattice nodes and change their direction with a probability taken from the histogram of angles in Fig. 3d. Two polar graphs are presented at each lattice point (Fig. 3e), comparing the measured (red) and predicted (blue) probabilities for axons to be oriented in given directions at that point (see Supplementary Information). The simulated trajectories are qualitatively similar to the measured ones. Quantitatively, the mean absolute value of the difference between the simulated and measured histograms is 40% and the correlation between the two is $R = 0.6$. The main difference is that the boundary layer (the region where axons are mostly parallel to the boundary) is wider in reality than in simulations. According to the simulation, the number of cells crossing forward is three times larger than the number of axons crossing backwards.

From the above simulations as well as from direct measurements of GFP images, we found that the number of axons crossing between triangles is asymmetrically distributed between the two possible directions of crossings. On average, we obtain that $M_{fwd} = 360$ neurons send their axons forward across the apex and into the triangle beyond it, whereas $M_{bwd} = 120$ neurons send their axons in the opposite direction (see Supplementary Information). In practice, only 20% of the diodes perform well, whereas the rest are closer to symmetrical transmission lines, so that daisy-chaining the triangles exponentially amplifies the probability for asymmetry in transmission (this production rate is determined by limitations of patterning and of axonal guidance, and should not be confused with functional reliability, which is 92% once they are produced).

THEORY AND COMPARISON WITH EXPERIMENT

To model the structure–function relation of a threshold device, we follow the approach of von Neumann[3] and assume that M input neurons are connected across the barrier onto one output

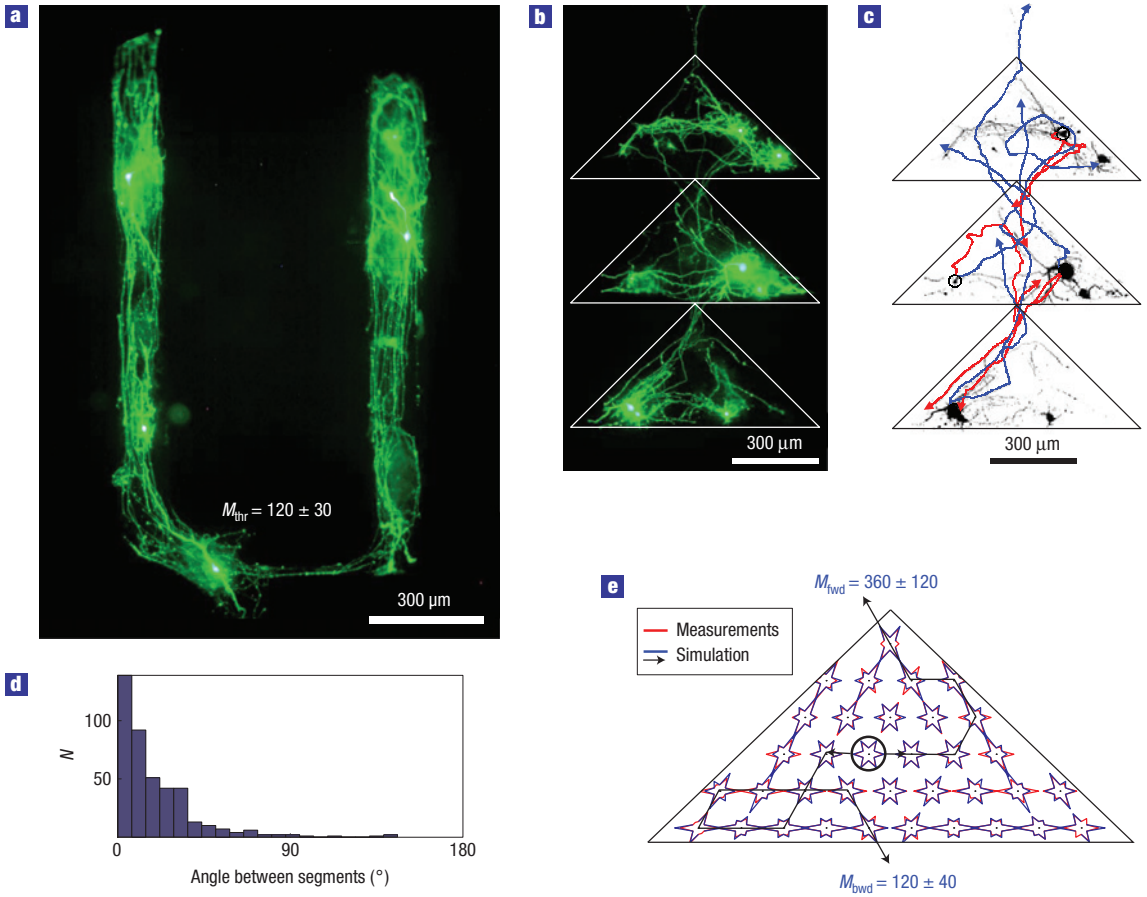

Figure 3 Internal structure of neuronal devices. a,**b**, Fluorescence images of devices transfected with non-specific GFP. Long and uniformly thin processes are axons. Bright spots are cell bodies (somas) and thick processes near the somas are dendrites. **a**, A threshold component: the average number of cells that send axons from one side of the thin obstruction to the other is 120±30 cells (see Supplementary Information). **b**, A diode: the average number of cells that send axons across triangles is 480±120 (see Supplementary Information). **c**, Manual tracing of all axons that cross between triangles in **b**. Circles mark the cell of origin of each axon; arrows mark the end of each axon. Blue coloured axons cross forward between triangles, whereas red coloured axons cross backwards. **d**, Histogram of angles measured from the GFP images between adjacent axonal steps the size of the simulation lattice (see Supplementary Information). The histogram is mirror symmetric around 0°. **e**, Computer simulation of axonal growth. Black: two simulated axonal paths. Blue: orientation histograms from computer simulation (see Supplementary Information). Red: orientation histograms measured from experimental GFP images of axons (integrated over 11 images). According to the simulation, the 480 cells that send axons across triangles (see **b**) divide into 360±120 cells crossing forward and 120±40 cells crossing backwards (see Supplementary Information).

neuron. We begin by describing the output unit as simply having a step-function response requiring a threshold of $m_o = 15 \pm 5$ input spikes to fire one output spike[7,15,18,19], and thereafter the number of spikes that it fires depends linearly on the number of inputs. The unreliability of the input is approximated by a binary variable, with an independent probability η of each spike to fail in transmitting a value of '1' (ref. 20). The probability to have n input spikes fail is therefore binomially distributed and can be approximated by a Gaussian to obtain a modified error function (see Supplementary Information). In a given burst, we denote by X the total number of spikes fired at the input and by Y the number of spikes that each output neuron fired:

$$Y = aX \cdot \phi\left(\frac{X - m_o'/(1-\eta)}{\sqrt{X\eta/(1-\eta)}}\right). \qquad (1)$$

As described in Supplementary Information, the linear part of equation (1) describes the increase of output firing when the number of input spikes is increased and the slope a is determined from the data. ϕ is the normal cumulative distribution function and $m_o' = m_o/(0.4C)$ accounts for the fact that 30% of the neurons are inhibitory[21] and includes a correction factor C that accounts for the degree of connectivity (not all M input neurons connect to the output neuron) and for losses due to asynchronous firing (see Supplementary Information). Intuitively, the output behaves as a modified threshold with a transition region that is shifted from m_o' because of η and the width of which is narrower, producing fewer errors, owing to the multiplexing factor M (see Supplementary Information).

In our experiments, we differentiate between four different 'modified threshold devices'. The thin section of each logic device constitutes a threshold device—we treat the AND gate as one doubly thick threshold ($M_{AND} = 2M_{thr} = 240$) and the diode as a combination of two modified thresholds—one backward and one forward.

We measure the normalized fluorescence amplitude α at the input region and the corresponding normalized output amplitude α^*. We scale both variables by M, the measured number of cells with axonal outputs that cross the device (see Fig. 3), to get $Y = \alpha^* M$ and $X = \alpha M$. Although the four types of modified

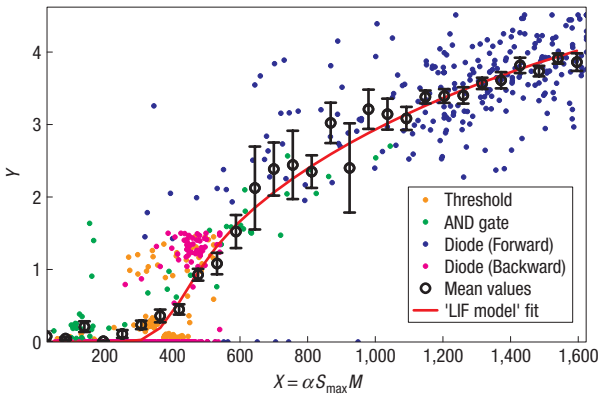

Figure 4 Error-correction model based on redundancy. The number of input spikes X fired in a specific burst versus the output response Y in units of spikes per neuron. The LIF model (red line, see text and Supplementary Information) was fitted using the experimentally measured burst events for all of the modified thresholds, averaged in 30 bins (large black circles, error bars mark the standard error for each binning value). Scaling of units in the model is explained in Supplementary Information. The fit parameters (with 95% confidence intervals) were: $\Delta T/t_{ref} = 7.6 \pm 1.1$, $m_o' = m_o/(0.4C) = 148 \pm 43$ and $\eta = 0.64 \pm 0.08$ with a correlation coefficient of $R^2 = 0.99$.

threshold device exhibit very different input–output relations, when plotting Y versus X we obtain a striking collapse of all the scaled data onto a single curve (Fig. 4). All devices exhibit the marked threshold transition at the same $X = X_t = 450$ spikes. According to the model, just beyond the threshold all neurons fire exactly one spike, so at the transition point, half of the output neurons fire once and we use this to rescale Y so that $Y(X_t) = 1/2$ spike per neuron. The full range of Y then occurs at an average maximal number of spikes per neuron $S_{max} = Y_{max} = 4.5$ spikes per neuron. As the characteristics of input and output neurons are the same, we rescale $X \to S_{max}X$, fixing in this way the parameter $a = Y_{max}/X_{max}$, where X_{max} is the maximal value of X.

To obtain an estimate for η, we improve the approximation of the neuronal output response, by using a leaky integrate and fire (LIF) model and by counting separately the number of inhibitory and excitatory input spikes that fail (see Supplementary Information). Solving the resulting finite sum numerically and fitting the data in Fig. 4 gives $m_o' = 148 \pm 43$ and $\eta = 0.64 \pm 0.08$. This value of η is in good agreement with direct measurements[20,22]. Taking $m_o = 15 \pm 5$ from the literature[7,15,18,19] we obtain: $C = 0.25 \pm 0.1$. Thus, losses due to a lack of synchrony or connectivity reduce the efficiency of excitation by a factor of four.

The model provides an estimate for the error rate ε of a threshold device (see Supplementary Information):

$$\varepsilon \approx \frac{\sqrt{X_t \eta/(1-\eta)}}{S_{max}M}. \qquad (2)$$

Inserting $X_t = 450$ spikes and $\eta = 0.64$ into equation (2), we get estimates of the error rate $\varepsilon = 5\%$, 5%, 3% and 1.5% for the threshold component, backward diode, AND gate and forward diode respectively. This compares well to measured error rates for each of the modified thresholds, which are $\varepsilon = 6\%$, 2%, 1.5% and 1% respectively (see Supplementary Information). Note that these error rates are related to but different from the error rates (given in Fig. 2) of the full AND gate and neuronal diode taken as logical devices. The errors are less than a tenth of the error η of the single axon. The improvement is the result of redundancy-based error correction[3].

EXTENSIONS

The devices also operate on the temporal character of the signal. Figure 5a shows that the threshold introduces a time delay as the signal rebuilds beyond the barrier, which is on average (95 ± 24 ms) but can reach a second for intermediate amplitudes. The AND gate introduces a coincidence detection with time resolution of around 100 ms. We can therefore foresee the construction of a multitude of complex logical and time-domain functional devices. For example, the directionality of the diode could be combined with the refractory period of the neuronal culture to create the NOT gate (Fig. 5c).

Refractoriness is overcome to create an oscillator as in Fig. 5b. The device is a 10 cm closed loop shaped as a pentagonal-cross with several neuronal diodes daisy-chained along the loop. Such a device cannot be constructed using only bi-directional transmission lines owing to the refractoriness—activity in a loop without diodes propagates in both directions but when the two fronts meet they annihilate (data not shown). A circumference of 10 cm ensures that when the activity completes a cycle, the neuron can fire again. A periodic behaviour of up to three cycles was measured (Fig. 5b). After traversing 24 cm the activity decayed, presumably owing to depletion of ionic resources. The oscillator can be used as a binary memory component and as a clock. In principle, a universal computing machine[23] can be constructed from the NAND, clock and memory components.

OUTLOOK

The logical functions achieved are direct results of the geometric constraints imposed and of a function-follows-structure architecture. In particular, we have seen that the existence of the threshold enables the establishment of logical gating functions. Gating with multiple inputs is indeed an inherent principle of neural computation[18]. In the nervous system, multiple inputs with a threshold for activation can be found, for example in temperature sensation[24], in propagation of activity within the hippocampus[25,26] and in the hearing system of the owl[27].

The surprisingly low reliability of inter-neuron connections within brain regions is a puzzle. Resource limitations in the brain can provide a partial explanation[28,29], but connections in the brain can also be very reliable[2,30–33]. Several reports have shown that the reliability of central nervous system synapses tends to increase at physiological temperatures[34], although others report no dependence[22]. An interesting proposal is that variable fidelity is a feasible and rapid mechanism for synaptic plasticity, for example, during learning or memory formation: tuning the synaptic reliability creates a large dynamic range of response[35,36]. In the hippocampus, it was already shown that learning changes the reliability rather than the strength of synapses[20]. Our model shows that even if m_o (which corresponds to synaptic strength) is left unchanged, then the threshold for response can be tuned by η (which corresponds to synaptic reliability[22]) with practically no change in overall error rate ε. Thus, by paying a 'redundancy price' of just 100 multiplexes, reliable devices are constructed from unreliable synaptic connections, the fidelity of which can be used as a tool to tune the devices' own function. In the future, it would be interesting to use the dependence of reliability on parameters such as calcium concentration or temperature to adjust the response of the devices, perhaps even to turn them on or off.

In comparison with electronic devices, these neuronal assemblies are bulky, slow and inefficient. In fact, there exist single

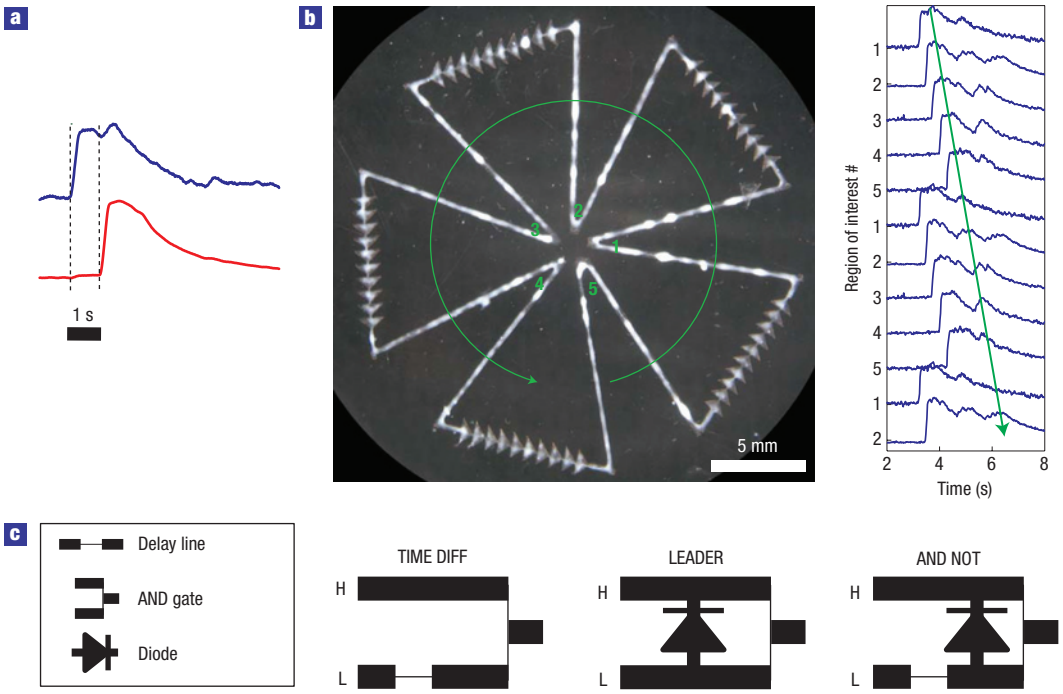

Figure 5 Complex devices. a, The temporal function of the threshold is a delay line. In the example, a delay of 1 s exists between the incoming signal (blue) and the outgoing signal (red) of a threshold device. **b**, Experimental implementation of a neuronal oscillator. Activity is measured in the five inner nodes that fit in the microscope's field of view. The time traces of fluorescence intensity are a replication of the same data from the five regions of interest to emphasize the propagating oscillations. A green arrow on the time traces follows a burst that completed 2.4 cycles around the oscillator. Amplitudes are scaled as in Fig. 2. **c**, Theoretical design of assembled devices. The TIME DIFF detects specific time difference between two inputs: only a signal H that lags behind signal L with a specific delay will elicit a response in the output. LEADER detects the order of arrival of two signals: a signal H that arrives before signal L imposes a refractory period in its transmission line, which blocks the later signal coming from L. Only when signal L precedes signal H can it travel beyond the diode and elicit an output response. The LEADER function can be modified to create the AND NOT gate, where the L signal controls the NOT H function, providing that both signals arrive simultaneously. If the control signal is always present at L (using the oscillator for example) then the gate can be modified into a NOT gate.

neurons in the brain that can carry out such computations on their own. However, we should keep in mind that both electric computation (the vacuum tube diode of Fleming and triode of De Forest) and more recently DNA computation[37] have their origin in bulky or cumbersome set-ups. We furthermore believe that computational circuits in neuronal cultures are interesting to study on their own, revealing how neurons behave when interacting in ensembles. The emergent property of computational power does not seem to arise in randomly connected neuronal cultures. Only when homogeneity is broken, using either 'blue prints' for connectivity (as we have demonstrated) or synaptic modulation in response to inputs[38], does computation appear. Studying *in vitro* cultures that carry out computation provides insight into the interplay of design and input, both relevant *in vivo*.

METHODS

COVERSLIP PATTERNING

Glass coverslips (13 mm diameter #1 Menzel Glaser) were patterned to make only specific locations available for cell adhesion[17]. Coverslips were first cleaned in 20% ammonium hydroxide and 20% hydrogen peroxide in double-distilled water (30 min at 50 °C). The non-adhesive substance used was Pluronics, which was attached to glass coverslips only by means of the following layers. Pluronics attaches to octadecanthiol, which attaches to gold, which attaches to chrome, which attaches well to the coverslips. We therefore coated the coverslips by evaporation of a 6 Å layer of chrome followed by a layer of 35 Å of gold and then immersion for 2 h in a solution of 0.1% octadecanthiol (Sigma-Aldrich) in ethanol (soluble through sonication for 15 min). Coverslips were then washed in ethanol, dried with nitrogen, immersed for 1 h in a solution of 3.5% Pluronics F108 Prill (BASF) in Dulbecco's PBS (soluble through stirring) and dried again.

An HP 7475A plotter (Hewlett–Packard), in which the pen was replaced by a sharp metal tip, was used to etch lines, rectangles and triangles through this coating, to create the finalized pattern as shown in Fig. 1. A Labview module was programmed to parse each line stored in a given text file into a long list of plotter commands so that each of the two-dimensional shapes is constructed by etching adjacent lines that form the shape, and repeating this procedure with perpendicular lines to ensure perfect clearing of the Pluronics in that area.

The coverslips were then sterilized under ultraviolet light for 10 min and incubated overnight in a solution of 3.5% Pluronics F108 Prill, 0.0028% laminin (Sigma-Aldrich) and 0.0028% fibronectin (Sigma-Aldrich), which form the cell adhesive layer. Finally, they were washed twice in Dulbecco's PBS and incubated again for several hours in plating medium before replacing the medium and plating the cells over it in fresh medium.

For details on culture of hippocampal neurons on patterned coverslips and imaging neuronal activity with calcium-sensitive fluorescent dyes, see Supplementary Information.

NETWORK STIMULATION

Local drug application was attained using a specially designated double-pipette system[17]. Local drug application as a means for excitation of signals has many advantages over electrical excitations[39,40], is more natural than global excitation and happens in the real brain. The system consists of two concentric pipettes of which the inner one—which has a 10 μm tip diameter and protrudes about 100 μm from the opening of the larger pipette—is used as a regular application pipette. The outer pipette has a tip diameter of about 100 μm and is constantly

under-pressurized, maintaining a steady suction of any surrounding liquid. This creates a very controllable and localized flow of the applied solution with no leakage to the surrounding cells.

For stimulation of the culture, the inner pipette was loaded with 200 μM L-glutamic acid buffered in recording medium. The flow was calibrated to reach an area with diameter of about 100 μm. Smaller perfusion areas were less likely to stimulate the network. Application times of between 20 ms and 1 s were used, typically 100 ms at a rate of once every 20 s. For local obstruction of the signal, the inner pipette was loaded with 1 μM of TTX, and the flow calibrated to reach an area with diameter of about 200 μm. The drug was continuously applied for periods up to ten minutes long.

The computational devices were also characterized using spontaneous activity in the cultures. In linear cultures, spontaneous bursts originate from initiation sites that are localized within a millimetre[8]. The causal burst propagation needed for proper function of the devices is therefore left uncompromised. The actual locations of burst initiation were determined offline. As verified on both threshold and diode devices, evoked and spontaneous bursts yield no apparent differences in device function.

DATA ANALYSIS

Error estimates given for fitted values are the 95% confidence limits, whereas for the measured data they are the standard error of the mean. Further information is given in Supplementary Information.

COMPUTER SIMULATIONS OF AXONAL GROWTH

To simulate axonal growth in the triangles, a simulation was carried out on a hexagonal lattice of N sites on the triangle. Neurons were placed on the lattice according to the physical location at which GFP fluorescent neurons were found, and the axons were then propagated. The axons advance from one node to any of its six neighbouring nodes with a probability that is set by the average measured probability of an axon to change its direction, as calculated by analysing the GFP images. The directional histograms of the simulated axons were then compared with the measured ones (for more details, refer to Supplementary Information).

The ratio of backward and forward crossings was calculated using a similar simulation in which the probability mentioned above of axonal advance was modified by the measured directional histograms at each lattice node. Neurons were evenly distributed on the lattice and axons were propagated until reaching the mean axonal length as measured from the GFP images. The number of forward and backward crossings was then counted and the ratio evaluated (for more details, refer to Supplementary Information).

For details on GFP transfections, see Supplementary Information.

STRUCTURE AND OPERATION OF THE DEVICES

The patterns used in this experiment included the threshold component, the AND gate and the neuronal diode.

Threshold components (Fig. 1d, left panel) were patterned with two parallel straight lines 250 μm thick, 1.6 mm long and 500 μm apart, connected to each other only at one end, through a perpendicular line with a thickness that was below 50 μm. Input signals of population activity (either stimulated or spontaneous) were observed at one of the lines and the resulting output signals were measured at the other line.

The AND gate (Fig. 1d, centre panel) was patterned with a pair of straight lines that served as inputs, spaced 950 μm apart and interconnected at one end with a thick perpendicular line. At the other end they were connected by two thin lines (50 μm thick and 350 μm long) to a central region serving as an output. Events were considered only if they initiated in either of the input regions. The thick connection between the two input regions was controlled with local application of TTX, which blocked the direct transmission of signals between the two lines. The two input regions fired independently when disconnected, and synchronously when connected.

In the diode, cultures were patterned into a series of concatenated isosceles triangles (1.4 mm wide and 650 μm high, Fig. 1d, right panel), each one connected at its tip to the base of the consecutive triangle. The input and output was measured from two consecutive triangles.

Received 25 March 2008; accepted 10 September 2008; published 12 October 2008.

References

1. Hopfield, J. J. Neural networks and physical systems with emergent collective computational abilities. *Proc. Natl Acad. Sci. USA* **79**, 2554–2558 (1982).
2. Movshon, J. A. Reliability of neuronal responses. *Neuron* **27**, 412–414 (2000).
3. von Neumann, J. in *Automata Studies* (eds Shannon, C. & McCarthy, J.) 43–98 (Princeton Univ. Press, 1956).
4. Jacobi, S. & Moses, E. Variability and corresponding amplitude-velocity relation of activity propagating in one-dimensional neural cultures. *J. Neurophysiol.* **97**, 3597–3606 (2007).
5. Eytan, D. & Marom, S. Dynamics and effective topology underlying synchronization in networks of cortical neurons. *J. Neurosci.* **26**, 8465–8476 (2006).
6. Reinagel, P., Godwin, D., Sherman, S. M. & Koch, C. Encoding of visual information by LGN bursts. *J. Neurophysiol.* **81**, 2558–2569 (1999).
7. Breskin, I., Soriano, J., Moses, E. & Tlusty, T. Percolation in living neural networks. *Phys. Rev. Lett.* **97**, 188102 (2006).
8. Feinerman, O., Segal, M. & Moses, E. Identification and dynamics of spontaneous burst initiation zones in uni-dimensional neuronal cultures. *J. Neurophysiol.* **97**, 2937–2948 (2007).
9. Marom, S. & Shahaf, G. Development, learning and memory in large random networks of cortical neurons: Lessons beyond anatomy. *Q. Rev. Biophys.* **35**, 63–87 (2002).
10. Wyart, C. *et al.* Constrained synaptic connectivity in functional mammalian neuronal networks grown on patterned surfaces. *J. Neurosci. Methods* **117**, 123–131 (2002).
11. Chang, J. C., Brewer, G. J. & Wheeler, B. C. Neuronal network structuring induces greater neuronal activity through enhanced astroglial development. *J. Neural Eng.* **3**, 217–226 (2006).
12. Chang, J. C., Brewer, G. J. & Wheeler, B. C. Modulation of neural network activity by patterning. *Biosens. Bioelectron.* **16**, 527–533 (2001).
13. Zeck, G. & Fromherz, P. Noninvasive neuroelectronic interfacing with synaptically connected snail neurons immobilized on a semiconductor chip. *Proc. Natl Acad. Sci. USA* **98**, 10457–10462 (2001).
14. Maher, M. P., Pine, J., Wright, J. & Tai, Y. C. The neurochip: A new multielectrode device for stimulating and recording from cultured neurons. *J. Neurosci. Methods* **87**, 45–56 (1999).
15. Feinerman, O., Segal, M. & Moses, E. Signal propagation along unidimensional neuronal networks. *J. Neurophysiol.* **94**, 3406–3416 (2005).
16. Feinerman, O. & Moses, E. Transport of information along unidimensional layered networks of dissociated hippocampal neurons and implications for rate coding. *J. Neurosci.* **26**, 4526–4534 (2006).
17. Feinerman, O. & Moses, E. A picoliter 'fountain-pen' using co-axial dual pipettes. *J. Neurosci. Methods* **127**, 75–84 (2003).
18. Stevens, C. F. Neuronal communication. Cooperativity of unreliable neurons. *Curr. Biol.* **4**, 268–269 (1994).
19. Thomson, A. M., Deuchars, J. & West, D. C. Large, deep layer pyramid-pyramid single axon EPSPs in slices of rat motor cortex display paired pulse and frequency-dependent depression, mediated presynaptically and self-facilitation, mediated postsynaptically. *J. Neurophysiol.* **70**, 2354–2369 (1993).
20. Stevens, C. F. & Wang, Y. Changes in reliability of synaptic function as a mechanism for plasticity. *Nature* **371**, 704–707 (1994).
21. Soriano, J., Rodríguez-Martínez, M., Tlusty, T. & Moses, E. Development of input connections in neural cultures. *Proc. Natl Acad. Sci. USA* **105**, 13758–13763 (2008).
22. Allen, C. & Stevens, C. F. An evaluation of causes for unreliability of synaptic transmission. *Proc. Natl Acad. Sci. USA* **91**, 10380–10383 (1994).
23. Turing, A. M. On computable numbers, with an application to the Entscheidungsproblem. *Proc. London Math. Soc.* **42**, 230–265 (1936).
24. Yarnitsky, D. & Ochoa, J. L. Differential effect of compression-ischaemia block on warm sensation and heat-induced pain. *Brain* **114**, 907–913 (1991).
25. Csicsvari, J., Hirase, H., Mamiya, A. & Buzsaki, G. Ensemble patterns of hippocampal CA3-CA1 neurons during sharp wave-associated population events. *Neuron* **28**, 585–594 (2000).
26. Andersen, P., Trommald, M. & Jensen, V. Low synaptic convergence of CA3 collaterals on CA1 pyramidal cells suggests few release sites. *Adv. Second Messenger Phosphoprotein Res.* **29**, 340–351 (1994).
27. Carr, C. E. Processing of temporal information in the brain. *Annu. Rev. Neurosci.* **16**, 223–243 (1993).
28. Laughlin, S. B., de Ruyter van Steveninck, R. R. & Anderson, J. C. The metabolic cost of neural information. *Nature Neurosci.* **1**, 36–41 (1998).
29. Varshney, L. R., Sjostrom, P. J. & Chklovskii, D. B. Optimal information storage in noisy synapses under resource constraints. *Neuron* **52**, 409–423 (2006).
30. Stratford, K. J., Tarczy-Hornoch, K., Martin, K. A., Bannister, N. J. & Jack, J. J. Excitatory synaptic inputs to spiny stellate cells in cat visual cortex. *Nature* **382**, 258–261 (1996).
31. Sterling, P. & Matthews, G. Structure and function of ribbon synapses. *Trends Neurosci.* **28**, 20–29 (2005).
32. Kara, P., Reinagel, P. & Reid, R. C. Low response variability in simultaneously recorded retinal, thalamic, and cortical neurons. *Neuron* **27**, 635–646 (2000).
33. MacLean, J. N., Watson, B. O., Aaron, G. B. & Yuste, R. Internal dynamics determine the cortical response to thalamic stimulation. *Neuron* **48**, 811–823 (2005).
34. Hardingham, N. R. & Larkman, A. U. Rapid report: The reliability of excitatory synaptic transmission in slices of rat visual cortex in vitro is temperature dependent. *J. Physiol.* **507**, 249–256 (1998).
35. Koch, C. *Biophysics of Computation: Information Processing in Single Neurons* (Oxford Univ. Press, 1999).
36. Smetters, D. K. & Zador, A. Synaptic transmission: Noisy synapses and noisy neurons. *Curr. Biol.* **6**, 1217–1218 (1996).
37. Adleman, L. M. Molecular computation of solutions to combinatorial problems. *Science* **266**, 1021–1024 (1994).
38. Shahaf, G. & Marom, S. Learning in networks of cortical neurons. *J. Neurosci.* **21**, 8782–8788 (2001).
39. Murphy, T. H., Blatter, L. A., Wier, W. G. & Baraban, J. M. Spontaneous synchronous synaptic calcium transients in cultured cortical neurons. *J. Neurosci.* **12**, 4834–4845 (1992).
40. Wu, J. Y., Guan, L. & Tsau, Y. Propagating activation during oscillations and evoked responses in neocortical slices. *J. Neurosci.* **19**, 5005–5015 (1999).

Supplementary Information accompanies the paper at www.nature.com/naturephysics.

Acknowledgements

We thank M. Segal, T. Tlusty, J.-P. Eckmann and S. Jacobi for stimulating discussions and V. Greenberger, J. Soriano and N. Ben-Sinai for their support. We acknowledge partial support by the Clore Center for Biological Physics, the Minerva Stiftung, Munich, Germany, by the Paedagogica Foundation and by the Israel Science Foundation under grant number 993/05.

Author information

Reprints and permissions information is available online at http://npg.nature.com/reprintsandpermissions. Correspondence and requests for materials should be addressed to A.R.